Nano Energy 66 (2019) 104124

Contents lists available at ScienceDirect

Nano Energy

journal homepage: http://www.elsevier.com/locate/nanoen

Communication

Hybrid nanomanufacturing of mixed-dimensional manganese oxide/graphene aerogel macroporous hierarchy for ultralight efficient supercapacitor electrodes in self-powered ubiquitous nanosystems

Chenxiang Ma [a,b], Ruoxing Wang [a,c], Halil Tetik [d], Shengjie Gao [a,c], Min Wu [a,c], Zhiyuan Tang [b], Dong Lin [d,**], Dong Ding [e,***], Wenzhuo Wu [a,c,*]

[a] School of Industrial Engineering, Purdue University, West Lafayette, IN, 47907, USA
[b] Department of Applied Chemistry, School of Chemical Engineering and Technology, Tianjin University, Tianjin, 300072, China
[c] Flex Laboratory, Purdue University, West Lafayette, IN, 47907, USA
[d] Department of Industrial and Manufacturing Systems Engineering, Kansas State University, Manhattan, KS, 66506, USA
[e] Energy & Environment Science and Technology, Idaho National Laboratory, Idaho Falls, ID, 83415, USA

ARTICLE INFO

Keywords:
Hybrid nanomanufacturing
Mixed-dimensional heterostructures
2-D MnO_2
3-D printed graphene aerogel
Ultralight supercapacitor electrodes
Self-powered ubiquitous nanosystems

ABSTRACT

The economic production of wearable energy storage devices exhibiting mechanically-compliable form factors and reliable performance enable exciting opportunities in emerging technologies of consumer electronics, human-machine interface, and the Internet of Things. Here we report a hybrid scheme for designing and nanomanufacturing ultralight, high-performance supercapacitor electrodes through the hydrothermal growth of two-dimensional MnO_2 on three-dimensional printed graphene aerogel (GA). The derived mixed-dimensional hierarchical macroporous composite electrodes exhibit superior specific capacitance and excellent cycling stability after thousands of cycles. We further explored the integration of a contact mode triboelectric nanogenerator and a mixed-dimensional MnO_2/GA based supercapacitor into a self-powered system that is capable of converting mechanical signals into electrical power and further storing such scavenged power. The holistic integration of energy harvesting and storage units promises the implementation of self-powered wearable devices with greater intelligence that can scavenge and store environmental energy through sustainable pathways for ubiquitous electronics in societally-pervasive applications.

1. Introduction

The economic production and integration of nanomaterials-based wearable energy storage devices exhibiting mechanically-compliable form factors and reliable performance will provide exciting opportunities in emerging technologies such as consumer electronics, pervasive computing, human-machine interface, robotics, and the Internet of Things (IoT) [1–10]. For continuous and efficient operation, the wearable energy storage units should ideally possess characteristics such as high energy density, lightweight, the capability to withstand large deformation [11–19]. Moreover, the holistic integration of appropriate energy harvesting and storage units promises the implementation of self-powered wearable devices with greater intelligence that can scavenge and store the environmental energy through sustainable pathways for sustainable onboard operations.

Electrochemical capacitors or supercapacitors (SCs) are power storage devices which store electric charge in the Faraday double layer on the electrode surfaces that are in contact with the electrolyte [20]. In this configuration, stable positive and negative double-layer will form at the solid-liquid interface [21,22]. To enhance the storage capacity in the supercapacitors, the electrodes are often modified with materials having better storage abilities of electric charge [23–27]. To this end, transition metal oxides have been intensively researched for potential use as the active materials [28–33]. For instance, manganese dioxide (MnO_2) with characteristics such as environmental friendliness and earth-abundance has been shown to possess high energy density and fast

* Corresponding author. School of Industrial Engineering, Purdue University, West Lafayette, IN, 47907, USA.
** Corresponding author.
*** Corresponding author.
E-mail addresses: dongl@ksu.edu (D. Lin), dong.ding@inl.gov (D. Ding), wenzhuowu@purdue.edu (W. Wu).

https://doi.org/10.1016/j.nanoen.2019.104124
Received 4 September 2019; Received in revised form 18 September 2019; Accepted 19 September 2019
Available online 23 September 2019

charge/discharge [34,35]. However, the rate capability and reversibility of MnO_2 electrodes are largely limited due to its extremely low electrical conductivity [36,37]. To address these issues, carbonaceous materials have been combined with MnO_2 to form composites with higher electrical conductivities and large specific surface areas [38–41]. These carbon materials provide continuous networks for electrical conduction and reduce impedance during cycling [42,43]. In previous studies [44,45], MnO_2-carbon composites were mainly prepared in powder form, which partly increases the specific capacitance of the active materials but is ineffective in reducing the device weight. Recently, the 3D printed graphene aerogel shows promise for serving as the backbone structures in lightweight MnO_2-carbon composites electrode with significantly boosted specific capacitance [19,46–49].

Herein, we report a hybrid scheme for designing and nano-manufacturing ultralight and high-performance supercapacitor electrodes through the hydrothermal growth of two-dimensional (2D) MnO_2 nanosheets on 3D printed macroporous graphene aerogel (GA)s. The derived mixed-dimensional hierarchical MnO_2/GA composite electrodes exhibit superior specific capacitance and excellent cycling stability after thousands of cycles. Compared to previous routes [50–53], the presented 3D printing template approach provides a more facile, economical, and controllable solution towards the realization of hierarchically porous graphene composites. We further presented a proof-of-concept demonstration of an integrated self-powered system that consists of a contact mode chitosan-based triboelectric nanogenerator (TENG) device [54] and the mixed-dimensional MnO_2/GA based supercapacitor. We showed that the integrated system is capable of converting mechanical signals into electrical power and further storing such scavenged power in the MnO_2/GA supercapacitor.

2. Results and discussion

The ultralight graphene aerogel was 3D printed following our reported procedures [47]. Unlike other approaches where the materials were heated up during printing or extruded out at room temperature [55,56], the cold plate in our 3D printing process rapidly freezes the water-based diluted graphene oxide suspension and selectively solidifies the aqueous droplets at −25 °C (Fig. 1a). During the freeze casting process, ice crystals grow along the temperature gradient, squeeze graphene nanosheets unidirectionally. The ice crystals are sublimated after freeze-drying, leaving interconnected micropores [47,57]. These micropores allow the manufacturing of MnO_2 nanosheets in the next step. Therefore, the water and low-viscosity graphene oxide suspension can be printed in a drop-on-demand mode, where the materials are ejected drop-by-drop digitally. Such digital fashion is different from the traditional 3D printing processes based on the continuous deposition [58], where the physical properties of the printed device can be affected by insufficient bond energy and surface voids formed during the intermolecular diffusion process [59,60]. In our printing process, the unfrozen material melts the frozen surface when the liquid solution is deposited on the previously frozen material. These two materials are mixed at low temperature (−25 °C) and then frozen together. Since the aqueous materials possess low viscosity after re-melting, the voids between layers will be filled by the liquid materials (i.e., graphene oxide suspension) subjected to surface tension and gravity. Compared to other advanced graphene aerogel printing technologies [61], the diluted graphene oxide suspension would provide the low density and large surface area for printing, and the final assembled graphene oxide can achieve high structural integrity and superior mechanical properties.

The process flow for manufacturing the mixed-dimensional hierarchical MnO_2/GA composite with the 3D printed GA as the skeleton is shown in Fig. 1. Briefly, the equimolar masses of $KMnO_4$ and HCl were first mixed in 40 ml deionized water with constant stirring for 1 h. The mixture was then added into a reactor that contained a graphene aerogel substrate and was placed in an oven at 85 °C for 6 h. The obtained product was washed and rinsed three times with deionized water and dried in a vacuum oven at 80 °C. Subsequently, the derived MnO_2/GA material was used to construct the electrodes. Fig. 1b shows an optical image of a MnO_2/GA electrode standing on a dandelion without any deformation of the stem, showcasing the ultra-lightweight nature of the mixed-dimensional MnO_2/GA composite. The cross-section scanning electron microscope (SEM) image of a MnO_2/GA electrode (Fig. 1c) clearly shows that the 2-D MnO_2 flakes grow uniformly with a high density on both sides of the graphene aerogel network.

We then studied the effects of the reaction conditions, e.g., growth temperature and time, on the growth outcome for 2-D MnO_2 flakes on GA. We found that the synthesis at 85 °C yields the optimal growth since MnO_2 cannot be successfully crystallized below 80 °C (Fig. S1a) and graphene aerogel substrate may not maintain its intact structure above 90 °C (Fig. S1b). We further explored and identified the optimal reaction time when the synthesis temperature was fixed at 85 °C. Fig. 2a shows the MnO2 flakes on GA with different reaction periods (3 h, 6 h, 9 h, and

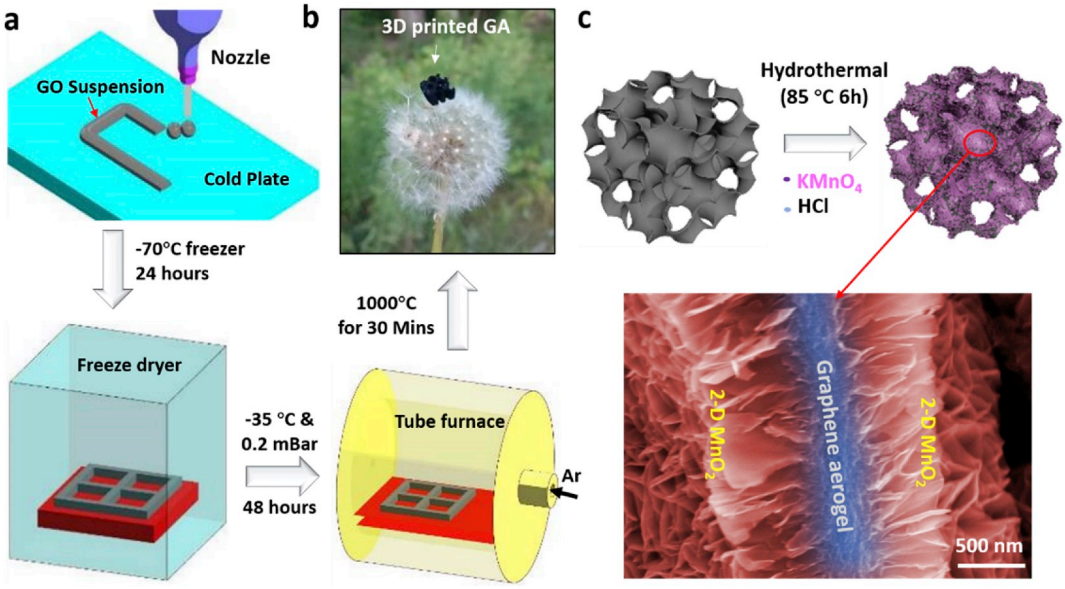

Fig. 1. Synthesis and fabrication process of MnO_2/GA electrode. (a) Scheme illustration of synthesis and fabrication process of MnO_2/GA electrode (b) Optical image of MnO_2/GA electrode standing on a dandelion without any deformation of the stem and (c) SEM image of MnO_2/GA electrode.

12 h). The three-hour synthesis yielded low-density MnO_2 flakes on the surface of graphene aerogel (Fig. 2a-1). With the reaction time increased to 6 h, the surface of graphene aerogel was fully covered by MnO_2 flakes with thin and uniform geometry. Compared to the bare GA framework, such high-density thin flakes provide a significantly enhanced specific surface area which is conducive to the contact with the electrolyte and hence benefits the surface oxidation-reduction reaction [62,63]. When the reaction time for MnO_2 growth was further increased to nine and twelve hours, a large amount of free-standing MnO_2 clusters accumulated around the specimens, which would have an adverse effect on the electrode performances [64]. We further characterized the galvanostatic charge-discharge (GCD) curves for MnO_2/GA samples with different reaction time at specific discharge currents of 2A g^{-1}, 5A g^{-1} and 10A g^{-1}, respectively, to reveal and compare the electrochemical performance of the electrodes prepared with different processing conditions (Fig. 2b, Fig. S2). The specific discharge capacities of the samples (at a specific discharge current of 2A g^{-1}) obtained with different reaction times are summarized in Fig. 2b. When the reaction time was 3 h, the specific capacitance of the product is only 94 F g^{-1}. When the reaction time was 6 h, the specific capacitance of the product could reach 213 F g^{-1}. With the increase of reaction time, the specific capacity of the products decreases, from 213 F g^{-1} to 158 F g^{-1} and 104 F g^{-1}. We have also tested the electrochemical impedance spectroscopy (EIS) curves of the MnO_2/GA samples obtained under different reaction time (Fig. S3) to differentiate their electrical conductivities. From the curves, MnO_2/GA samples obtained under different reaction time (3 h, 6 h, 9 h, and 12 h) have the same R_0, which means four conditions samples have similar ohmic resistance. Meanwhile, With the increase of reaction time, the radius of semi-circle in the high-frequency region becomes larger, which reflects the increase of electrochemical impedance. The reason should be that the electrical conductivities were reduced by the growth of MnO2 flake. However, when the reaction time is 12 h, MnO_2/GA sample has a lower slope, with the reason that excessive MnO_2 flake significantly increased concentration polarization. The results from the electron micrographs, GCD and EIS characterizations all suggest that the optimal synthesis condition for the growth of 2-D MnO_2 flakes on the surface of graphene aerogels is at 85 °C for 6 h.

Subsequently, we analyzed the material and structural properties of the samples obtained with the optimal conditions, using Energy-dispersive X-ray spectrometry (EDS) mapping analysis, Raman spectroscopy, and X-ray diffraction (XRD). Fig. S4 shows the elemental mapping for the MnO_2/GA sample, indicating that the Mn and O elements distribute uniformly on the surface of graphene aerogels. Fig. 2c shows the comparison of the Raman spectra for the MnO_2/GA samples and the bare graphene aerogel skeleton. In both the spectra, the D-band at 1358 cm^{-1} and G-band at 1596 cm^{-1} indicate the presence of graphene in the structure [65,66]. As shown in Fig. 2c, three Raman bands located at 514, 567, and 641 cm^{-1} for the MnO_2 flakes are in good agreement with the major vibrational features of Mn-O in the lattice vibration of α-MnO_2 [67–69]. The XRD pattern of the MnO_2/GA sample is shown in Fig. 2d, where the broadening of the XRD peaks is likely due to the existence of graphene with amorphous structure [70]. The peaks corresponding to the (110) crystal plane of manganese dioxide has the largest intensity and a relatively sharp profile. The (110) crystal plane of MnO_2 has a high surface energy [71,72] that can promote the reaction rate in the electrochemical process of supercapacitors, and hence improve the performance of the electrode.

We further performed cyclic voltammetry (CV) for the bare graphene aerogel framework and the mixed-dimensional hierarchical MnO_2/GA composite electrodes in three-electrode configurations (Fig. 3a). The specific capacitance of the MnO_2/GA electrodes increased significantly compared to that of the bare GA framework, which could be attributed to the pseudocapacitance from the 2-D manganese dioxide flakes. Meanwhile, the (110) surfaces of manganese dioxide have high energy and hence enhanced activity promoting the redox reaction [73,74]. The ultra-high surface area and conductivity of graphene aerogels backbones provide enhanced contact and electronic conductivity that further facilitate the redox processes on the surfaces of 2-D MnO_2 [75]. Fig. 3b shows the CV curves of MnO_2/GA electrodes in the potential window ranging from 0 to 0.8 V at different scan rates (10 mV s^{-1}, 20 mV s^{-1}, 50 mV s^{-1}, and 100 mV s^{-1}, respectively). Our mixed-dimensional hierarchical MnO_2/GA electrodes presented a stable structure and high conductivity that help stabilize the electrochemical performance under high-rate charge and discharge conditions [76]. As shown in Fig. 3b, with the scan rate increased, the rectangular-shaped CV curves for the MnO_2/GA electrodes remained unchanged, manifesting a stable cycling

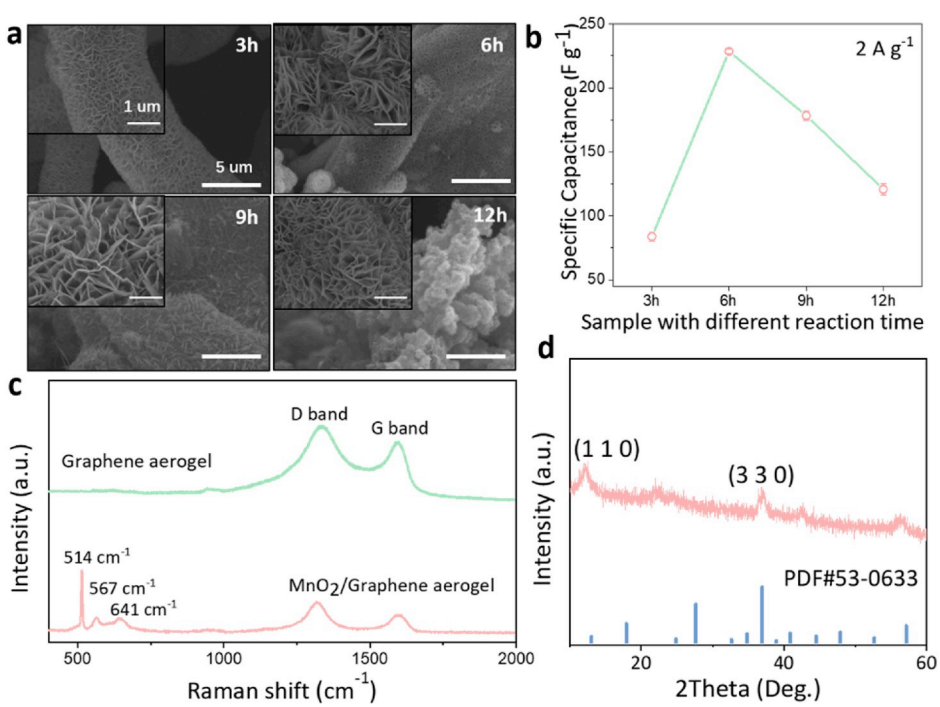

Fig. 2. MnO_2/GA electrode characterization (a) SEM images of MnO_2/GA samples with different reaction time (3 h, 6 h, 9 h and 12 h) (b) Specific discharge capacities of the MnO_2/GA samples obtained under different reaction time (3 h, 6 h, 9 h and 12 h) at a specific discharge current of 2A g^{-1} (c) EDX of the optimum product obtained at 85 °C for 6 h (d) Raman spectra of MnO_2/GA sample grown under optimal conditions and graphene aerogel template (e) XRD pattern of MnO_2/GA sample.

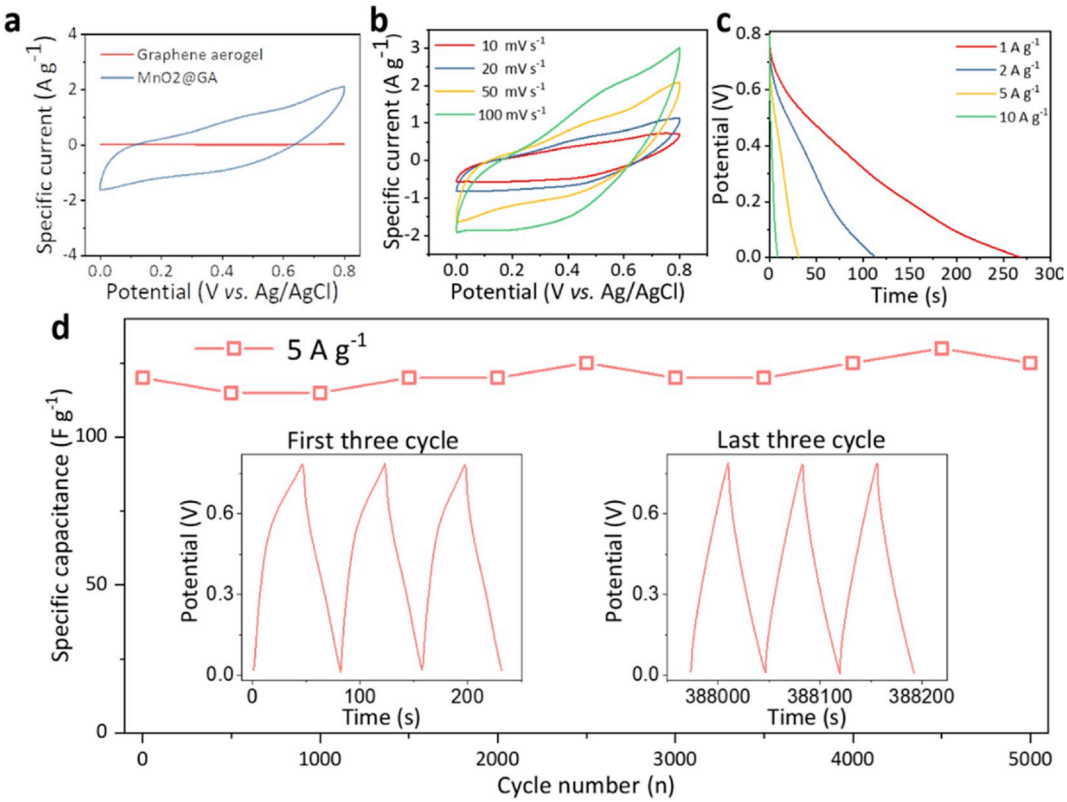

Fig. 3. Electrochemical performance of MnO_2/GA electrode. (a) Cyclic voltammetry of graphene aerogel templates and MnO_2/GA electrode in a three-electrode configuration (b) Cyclic voltammetry curves of MnO_2/GA electrodes in the potential window of 0–0.8 V at different scan rates (10 mV s^{-1}, 20 mV s^{-1}, 50 mV s^{-1} and 100 mV s^{-1}, respectively) (c) The discharge curves of MnO_2/GA electrodes at discharge specific currents of 1A g^{-1}, 2A g^{-1}, 5A g^{-1} and 10A g^{-1}, respectively (d) Cyclic performance of the MnO_2/GA electrode under 5 A g^{-1} charge and discharge current.

and satisfactory capacitive behavior [41,76]. Fig. 3c shows the discharge curves of the MnO_2/GA electrodes at discharge specific currents of 1 A g^{-1}, 2 A g^{-1}, 5 A g^{-1}, and 10 A g^{-1}. The discharge-specific capacitance of the MnO_2/GA electrode reached 275 F g^{-1} when the discharge specific current is 1 A g^{-1}. When the discharge specific current was increased to 10 A g^{-1}, the discharge specific capacitance of the MnO_2/GA electrodes still maintained at 90 F g^{-1}. To further characterize the cyclic stability for potential long-term practical applications, we measured the specific capacitance of the MnO_2/GA electrodes at the charge/discharge specific current of 5 A g^{-1} for 5000 cycles (Fig. 3d). After 5000 cycles, the specific capacitance of the MnO_2/GA electrodes did not decay but instead increased slightly, likely due to the porous nature of the graphene aerogels [77,78]. During the cycling, the electrolyte constantly wet the electrode surface and gradually infiltrated through the macroporous GA framework, hence increasing the contact area between the electrode and electrolyte and leading to improved material performance [79]. We have also included a benchmarking comparison between the performance of our MnO_2/GA electrode with those in the reported work (Supplementary Table 1).

The integration of flexible energy harvesting and energy storage units into a self-powered system promises the implementation of self-sustainable wearable devices with greater intelligence that can store the harvested electric power for other onboard operations [80–83]. The triboelectric nanogenerator (TENG) emerges as a promising technology for effectively scavenging the ubiquitous mechanical energy into electric power through the contact electrification and electrostatic induction [84–91]. Here, to develop the self-powered system that consists of the TENG energy harvester and the energy storage unit, we integrated the 3D printed MnO_2/GA supercapacitor on the same substrate with a TENG device made of biopolymer derived materials [54]. An optical image of the integrated device is shown in Fig. 4a, where the TENG incorporated a copper foil as the current collector and a chitosan film as the dielectric layer. The solid-state supercapacitor consisted of the 3D printed MnO_2/GA as the electrode and polyvinyl alcohol/lithium chloride (LiCl/PVA) gel as the electrolyte and separator [92].

We first characterized the electrochemical performance of the 3D printed MnO_2/GA supercapacitors. The electrochemical impedance spectroscopy (EIS) results for the device and its simulated equivalent circuit are shown in Fig. S5. Leveraging the ultrahigh conductivity of the three-dimensional graphene aerogel, the 3D printed MnO_2/GA supercapacitor exhibited an appealing internal resistance around 2 Ohms and the corresponding electrochemical impedance was 10 Ohms. Fig. 4b shows the discharge curves of the 3D printed MnO_2/GA supercapacitor with discharge specific currents of 1 A g^{-1}, 2 A g^{-1}, 5 A g^{-1}, and 10 A g^{-1}. The discharge-specific capacitance of the 3D printed MnO_2/GA supercapacitor reached 95 F g^{-1} with a discharge current of 1 A g^{-1}. At discharge specific current of 10 A g^{-1}, the discharge specific capacitance of the MnO_2/GA electrode maintained at 45 F g^{-1}. The energy and power densities were also calculated from GCD curves. The maximum energy density of 21 Wh/kg is achieved at a power density of 800 W/kg, while the highest power density is 36 kW/kg at the energy density of 10 Wh/kg. Fig. S6 exhibits the cyclic performance of the device with a 5 A g^{-1} discharge current. The 3D MnO_2/GA supercapacitor reached an initial specific capacitance of 80 F g^{-1} and maintained at 63 F g^{-1} even after 1000 cycles of operations. We further characterized the performance of the TENG module for converting the mechanical inputs into electrical power (details in SI). Fig. 4c shows the measured open-circuit voltage (V_{OC}) (~40 V), short-circuit current (I_{SC}) (~0.15 μA), and transfer charge (σ_{sc}) (~24 nC). The direct electrical outputs from the TENG should be rectified for properly charging the energy storage units [93,94]. Fig. 4d shows the rectified current waveform from the TENG through a rectifier circuit (Fig. S7). Moreover, we characterized the

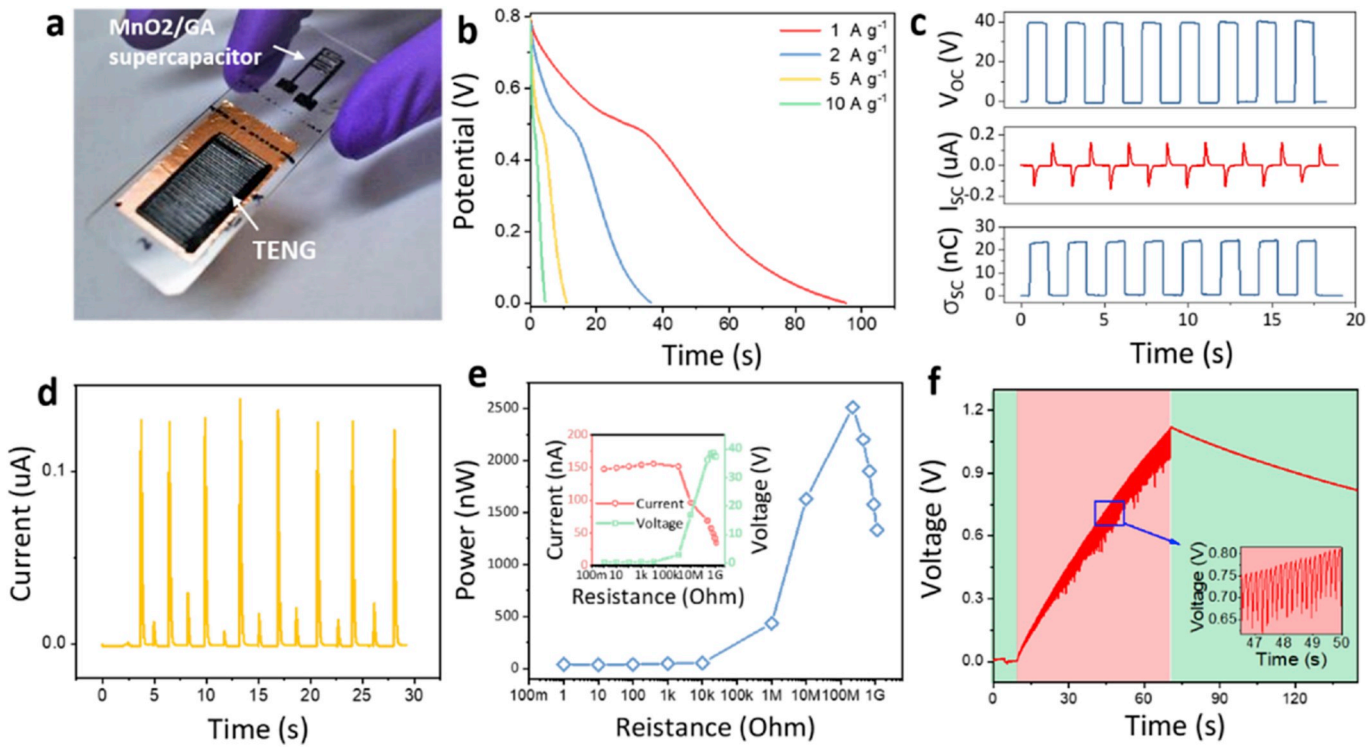

Fig. 4. Self-powered ubiquitous nanosystem. (a) Optical images of integrated self-power system (b) Discharge curves of 3D printed MnO_2/GA supercapacitor at discharge specific currents of 1A g^{-1}, 2A g^{-1}, 5A g^{-1} and 10A g^{-1}, respectively (c) electric performance of the TENG device (d) Current signal of CC-TENG device after rectification (e) power output of CC-TENG was characterized with different resistive loads (f) TENG charges the supercapacitor.

output power from the TENG module delivered to the external resistive loads (Fig. 4e). The highest instantaneous power output delivered to the load was estimated to be 2.5 μW when the external load matches the internal impedance of the TENG module (~200 M Ohm here) [95,96]. For a proof-of-concept demonstration, we used finger pressing as the mechanical inputs that can be effectively harvested by the TENG module, and the harvested energy was further used to charge the 3D MnO_2/GA supercapacitor (Fig. 4f). When the TENG was pressed by the human finger, the 3D MnO_2/GA supercapacitor became charged with 1.0 V in 60 s. The voltage change in the supercapacitor during the pressing process is shown in the enlarged figure. The voltage in the supercapacitor stabilized at 0.8 V subsequently, providing a reliable electrical source for the operations of other onboard electronics.

3. Conclusions

In summary, we have demonstrated a hybrid scheme for designing and nanomanufacturing mixed-dimensional ultralight macroporous hierarchy for efficient supercapacitor electrodes, through the hydrothermal growth of 2-D MnO_2 nanosheets on 3-D printed graphene aerogel with interconnected micropores. The derived mixed-dimensional hierarchical MnO_2/GA composite electrodes exhibit superior specific capacitance (275 F g^{-1}) and excellent cycling stability after thousands of cycles. We further presented a proof-of-concept demonstration of an integrated self-powered system that consists of a contact mode chitosan-based TENG device [54] and the mixed-dimensional MnO_2/GA based supercapacitor. We showed that the integrated system is capable of converting mechanical signals into electrical power and further storing such scavenged power in the MnO_2/GA supercapacitor for other onboard applications. Our work presents an important step towards the realization of self-powered nanosystems.

Author contributions

W. Z. W. and C. X. M. conceived the idea and wrote the manuscript. H.T. and D. L. prepared the graphene aerogel. C.X.M. fabricated the devices, performed the electrochemical test, and analyzed the data. C. X. M., S. J. G., and M. W. performed the system demonstration. C. X. M and R. X. W perform data analysis. W. Z. W. and D. D. guided the experiments for supercapacitor characterization. All authors have discussed the results and commented on the paper.

Acknowledgment

W. Z. W. acknowledges the College of Engineering and School of Industrial Engineering at Purdue University for the startup support and the Ravi and Eleanor Talwar Rising Star Assistant Professorship. The support provided by the China Scholarship Council (CSC) during a visit of Chenxiang Ma to Purdue University is acknowledged. L. D thanks the support from the National Science Foundation under Award No. OIA-1656006 and matching support from the State of Kansas through the Kansas Board of Regents and the support from Johnson Cancer Center. Part of this work was supported by a subcontract from the Idaho National Laboratory Directed Research and Development Program under DOE Idaho Operations Office Contract DE-AC07-05ID14517.

Appendix A. Supplementary data

Supplementary data to this article can be found online at https://doi.org/10.1016/j.nanoen.2019.104124.

References

[1] Z.L. Wang, W. Wu, Angew. Chem. Int. Ed. 51 (2012) 11700–11721.
[2] Q. Zheng, Y. Zou, Y. Zhang, Z. Liu, B. Shi, X. Wang, Y. Jin, H. Ouyang, Z. Li, Z. L. Wang, Sci. Adv. 2 (2016) e1501478.
[3] J.A. Rogers, T. Someya, Y. Huang, Science 327 (2010) 1603–1607.

[4] Y. Liu, M. Pharr, G.A. Salvatore, ACS Nano 11 (2017) 9614–9635.
[5] N.A. Kyeremateng, T. Brousse, D. Pech, Nat. Nanotechnol. 12 (2016) 7.
[6] D. Dickey Michael, Adv. Mater. 29 (2017) 1606425.
[7] X. Pu, M. Liu, X. Chen, J. Sun, C. Du, Y. Zhang, J. Zhai, W. Hu, Z.L. Wang, Sci. Adv. 3 (2017) e1700015.
[8] W. Liu, M.-S. Song, B. Kong, Y. Cui, Adv. Mater. 29 (2017) 1603436.
[9] J. Xiong, P. Cui, X. Chen, J. Wang, K. Parida, M.-F. Lin, P.S. Lee, Nat. Commun. 9 (2018) 4280.
[10] T. Someya, Z. Bao, G.G. Malliaras, Nature 540 (2016) 379.
[11] W. Yan, Z. Shi, H. Yi, Y. Ma, C. Wang, M. Chen, Y. Chen, J. Phys. Chem. C 113 (2009) 13103–13107.
[12] C. Liu, Z. Yu, D. Neff, A. Zhamu, B.Z. Jang, Nano Lett. 10 (2010) 4863–4868.
[13] W. Wei, X. Cui, W. Chen, D.G. Ivey, Chem. Soc. Rev. 40 (2011) 1697–1721.
[14] R. Genc, M.O. Alas, E. Harputlu, S. Repp, N. Kremer, M. Castellano, S.G. Colak, K. Ocakoglu, E. Erdem, Sci. Rep. 7 (2017) 11222.
[15] Z. Lei, X. Hu, Z. Wang, F. Sun, D.G. Dorrell, Renew. Sustain. Energy Rev. 81 (2017). S1364032117309292.
[16] Y. Yang, Q. Huang, L. Niu, D. Wang, C. Yan, Y. She, Z. Zheng, Adv. Mater. 29 (2017) 1606679.
[17] Q. Meng, K. Cai, Y. Chen, L. Chen, Nano Energy 36 (2017) 268–285.
[18] S. Wang, N. Liu, J. Su, L. Li, F. Long, Z. Zou, X. Jiang, Y.H. Gao, ACS Nano 11 (2017) 2066.
[19] L. Bao, T. Li, S. Chen, C. Peng, L. Li, Q. Xu, Y. Chen, E. Ou, W. Xu, Small 13 (2017).
[20] B. E. Conway, 1991.
[21] K.H. Chew, Y. Ishibashi, F.G. Shin, H.L.W. Chan, J. Phys. Soc. Jpn. 72 (2003) 2364–2368.
[22] T. Wandlowski, R.D. Levie, J. Electroanal. Chem. 345 (1993) 413–432.
[23] L.L. Zhang, X.S. Zhao, Chem. Soc. Rev. 38 (2009) 2520–2531.
[24] L.Q. Mai, Y. Fan, Y.L. Zhao, X. Xu, X. Lin, Y.Z. Luo, Nat. Commun. 2 (2011) 381.
[25] V. Strauss, K. Marsh, M.D. Kowal, M. Elkady, R.B. Kaner, Adv. Mater. 30 (2018) 1704449.
[26] P. Ji, J. Wan, Y. Xi, Y. Guan, C. Zhang, X. Gu, J. Li, J. Lu, D. Zhang, Nanotechnology 30 (2019) 335401.
[27] M.S. Javed, S. Dai, M. Wang, D. Guo, L. Chen, X. Wang, C. Hu, Y. Xi, J. Power Sources 285 (2015) 63–69.
[28] Z. Wu, Y. Zhu, X. Ji, C.E. Banks, Transition Metal Oxides as Supercapacitor Materials, 2016.
[29] R.R. Salunkhe, Y.V. Kaneti, Y. Yamauchi, ACS Nano 11 (2017) 5293.
[30] G. Yu, X. Xing, L. Pan, Z. Bao, C. Yi, J. Nanoen, Nano Energy 2 (2013) 213–234.
[31] T. Wei, M. Zhang, P. Wu, Y.J. Tang, S.L. Li, F.C. Shen, X.L. Wang, X.P. Zhou, Y. Q. Lan, Nano Energy 34 (2017) 205–214.
[32] Z. Xuan, J. Luo, P. Tang, X. Ye, X. Peng, H. Tang, S.G. Sun, J. Fransaer, Nano Energy 31 (2017) 311–321.
[33] C. Wang, Y. Xi, M. Wang, C. Zhang, X. Wang, Q. Yang, W. Li, C. Hu, D. Zhang, Nano Energy 28 (2016) 115–123.
[34] A.P.P. Alves, R. Koizumi, A. Samanta, L.D. Machado, A.K. Singh, D.S. Galvao, G. G. Silva, C.S. Tiwary, P.M. Ajayan, Nano Energy 31 (2017) 225–232.
[35] Tao Dong, Meng Li, Peng Wang, Ping Yang, Synthesis of hierarchical tube-like yolk-shell Co_3O_4@ $NiMoO_4$ for enhanced supercapacitor performance, Int. J. Hydrogen Energy 43 (31) (2018) 14569–14577.
[36] P.Y. Chan, Rusi, S.R. Majid, Solid State Ion. 262 (2014) 226–229.
[37] Z. Li, Y. Mi, X. Liu, L. Sheng, S. Yang, J. Wang, J. Mater. Chem. 21 (2011) 14706–14711.
[38] S. P. Muhammed, J. K. Vishal and A. C. Bose, 2016.
[39] J. Yan, Z. Fan, T. Wei, W. Qian, M. Zhang, F. Wei, Carbon 48 (2010) 3825–3833.
[40] Y. He, W. Chen, X. Li, Z. Zhang, J. Fu, C. Zhao, E. Xie, ACS Nano 7 (2013) 174.
[41] G.E. Jin, Y. Hong-Bin, H.U. Wei, Y.U. Xiao-Fang, Y. You-Xian, M. Li-Bo, L.I. Hui-Hui, L.I. Shan-Shan, Y.U. Shu-Hong, Nano Energy 2 (2013) 505–513.
[42] H. Wang, Z. Xu, Z. Li, K. Cui, J. Ding, A. Kohandehghan, X. Tan, B. Zahiri, B. C. Olsen, C.M.B. Holt, Nano Lett. 14 (2014) 1987–1994.
[43] M.S. Javed, J. Chen, L. Chen, Y. Xi, C. Zhang, B. Wan, C. Hu, J. Mater. Chem. 4 (2016) 667–674.
[44] G. Yu, L. Hu, N. Liu, H. Wang, M. Vosgueritchian, Y. Yang, Y. Cui, Z. Bao, Nano Lett. 11 (2015) 4438.
[45] X. Dong, X. Wang, W. Jing, S. Hao, X. Li, L. Wang, M.B. Chan-Park, M.L. Chang, C. Peng, Carbon 50 (2012) 4865–4870.
[46] B. Yao, S. Chandrasekaran, J. Zhang, W. Xiao, F. Qian, C. Zhu, E.B. Duoss, C. M. Spadaccini, M.A. Worsley, Y. Li, Joule 3 (2019) 459–470.
[47] Q. Zhang, F. Zhang, S.P. Medarametla, H. Li, C. Zhou, D. Lin, Small 12 (2016) 1702–1708.
[48] H. Hu, Z. Pei, H. Fan, C. Ye, Small 12 (2016) 3059–3069.
[49] K. Shen, J. Ding, S. Yang, Adv. Energy Mater. 8 (2018) 1800408.
[50] L. Peng, X. Peng, B. Liu, C. Wu, Y. Xie, G. Yu, Nano Lett. 13 (2013) 2151–2157.
[51] X. Dong, X. Wang, J. Wang, H. Song, X. Li, L. Wang, M.B. Chan-Park, C.M. Li, P. Chen, Carbon 50 (2012) 4865–4870.
[52] Y. Zhao, W. Ran, J. He, Y. Huang, Z. Liu, W. Liu, Y. Tang, L. Zhang, D. Gao, F. Gao, Small 11 (2015) 1310–1319.
[53] C. Xiong, T. Li, A. Dang, T. Zhao, H. Li, H. Lv, J. Power Sources 306 (2016) 602–610.
[54] R. Wang, S. Gao, Z. Yang, Y. Li, W. Chen, B. Wu, W. Wu, Adv. Mater. (2018), https://doi.org/10.1002/adma.201706267, 1706267.
[55] C.X.F. Lam, X.M. Mo, S.H. Teoh, D.W. Hutmacher, Mater. Sci. Eng. C 20 (2002) 49–56.
[56] M.S. Mannoor, Z. Jiang, T. James, L.K. Yong, K.A. Malatesta, W.O. Soboyejo, N. Verma, D.H. Gracias, M.C. Mcalpine, Nano Lett. 13 (2013) 2634–2639.
[57] P. Yan, E. Brown, Q. Su, J. Li, J. Wang, C. Xu, C. Zhou, D. Lin, Small 13 (2017).
[58] A.T. Miller, D.L. Safranski, C. Wood, R.E. Guldberg, K. Gall, J. Mech. Behav. Biomed. Mater. 75 (2017) 1–13.
[59] X. Lin, H. Liu, S.O. Architecture, Acta Opt. Sin. 36 (2016) 0816002.
[60] Wei Zhu, Kathryn R. Tringale, Sarah A. Woller, Shangting You, Susie Johnson, Haixu Shen, Jacob Schimelman, et al., Rapid continuous 3D printing of customizable peripheral nerve guidance conduits, Mater. Today 21 (9) (2018) 951–959.
[61] C. Zhu, Y.J. Han, E.B. Duoss, A.M. Golobic, J.D. Kuntz, C.M. Spadaccini, M. A. Worsley, Nat. Commun. 6 (2015) 6962.
[62] A. Gigot, M. Fontana, C.F. Pirri, P. Rivolo, Materials 11 (2018) 57.
[63] L. Liu, Y. Yan, Z. Cai, S. Lin, X. Hu, Adv. Mater. Interfaces (2018) 1701548.
[64] D. Gueon, J.H. Moon, Acs Sustain. Chem. 5 (2017).
[65] A.C. Ferrari, J.C. Meyer, V. Scardaci, C. Casiraghi, M. Lazzeri, F. Mauri, S. Piscanec, D. Jiang, K.S. Novoselov, S. Roth, Phys. Rev. Lett. 97 (2006) 187401.
[66] A.C. Ferrari, Solid State Commun. 143 (2007) 47–57.
[67] S. Jana, S. Pande, A.K. Sinha, S. Sarkar, M. Pradhan, M. Basu, S. Saha, T. Pal, J. Phys. Chem. C 113 (2009) 1386–1392.
[68] A. Kumar, A. Sanger, A. Kumar, Y. Kumar, R. Chandra, Electrochim. Acta 220 (2016) 712–720.
[69] J. Luo, H.T. Zhu, H.M. Fan, J.K. Liang, H.L. Shi, G.H. Rao, J.B. Li, Z.M. Du, Z. X. Shen, J. Phys. Chem. C 112 (2008) 12594–12598.
[70] X.C. Xiao, W.H. Jiang, L.X. Song, J.F. Tian, X.F. Hu, Diam. Relat. Mater. 9 (2000) 1782–1785.
[71] L.R. Pahalagedara, S. Dharmarathna, C.K. King'Ondu, M.N. Pahalagedara, Y. Meng, C.H. Kuo, S.L. Suib, J. Phys. Chem. C (2014) 118.
[72] X. Dong, W. Shen, J. Gu, L. Xiong, Y. Zhu, H. Li, J. Shi, J. Phys. Chem. B 110 (2006) 6015–6019.
[73] H. Jiang, C. Li, T. Sun, J. Ma, Chem. Commun. 48 (2012) 2606–2608.
[74] X. Zhao, G. Wang, G. Zhai, H. Wang, Chemistry 23 (2017) 7037.
[75] Y. Yang, B. Zeng, J. Liu, Y. Long, N. Li, Z. Wen, Y. Jiang, Mater. Res. Innov. 20 (2015) 92–98.
[76] S.L. Kim, J.H. Hsu, C. Yu, Nano Energy 48 (2018). S221128551830243X.
[77] L.J. Hoon, P. Nokyoung, K. Byung Gon, J. Dae Soo, I. Kyuhyun, H. Jaehyun, C. Jang Wook, ACS Nano 7 (2013) 9366–9374.
[78] Y. Yoon, K. Lee, C. Baik, H. Yoo, M. Min, Y. Park, S.M. Lee, H. Lee, Adv. Mater. 25 (2013) 4437–4444.
[79] X. Fei, W. Shuang, M. Wang and J. Wang, 2018, 190, 156-163.
[80] X. Pu, L. Li, H. Song, C. Du, Z. Zhao, C. Jiang, G. Cao, W. Hu, Z.L. Wang, Adv. Mater. 27 (2015) 2472–2478.
[81] J. Wang, X. Li, Y. Zi, S. Wang, Z. Li, L. Zheng, F. Yi, S. Li, Z.L. Wang, Adv. Mater. 27 (2015) 4830–4836.
[82] J. Zou, M. Zhang, J. Huang, J. Bian, Y. Jie, M. Willander, X. Cao, N. Wang, Z. L. Wang, Adv. Energy Mater. 8 (2018) 1702671.
[83] Q. Jiang, C. Wu, Z. Wang, A.C. Wang, J.-H. He, Z.L. Wang, H.N. Alshareef, Nano Energy 45 (2018) 266–272.
[84] G.Q. Gu, C.B. Han, J.J. Tian, T. Jiang, C. He, C.X. Lu, Y. Bai, J.H. Nie, Z. Li, Z. L. Wang, Nano Res. (2018) 1–12.
[85] H. Guo, X. Jia, L. Liu, X. Cao, N. Wang, Z.L. Wang, ACS Nano 12 (2018) 3461–3467.
[86] X. Yi, W. Jie, Y. Zi, X. Li, C. Han, C. Xia, C. Hu, Z. Wang, Nano Energy 38 (2017) 101–108.
[87] J. Chen, H. Guo, Z. Wu, G. Xu, Y. Zi, C. Hu, Z.L. Wang, Nano Energy 64 (2019) 103920.
[88] Z. Lin, B. Zhang, H. Guo, Z. Wu, H. Zou, J. Yang, Z.L. Wang, Nano Energy 64 (2019) 103908.
[89] G. Zhao, Y. Zhang, N. Shi, Z. Liu, X. Zhang, M. Wu, C. Pan, H. Liu, L. Li, Z.L. Wang, Nano Energy 59 (2019) 302–310.
[90] J. Luo, Z.L. Wang, Energy Storage Materials, 2019.
[91] M. Zhao, J. Nie, H. Li, M. Xia, M. Liu, Z. Zhang, X. Liang, R. Qi, Z.L. Wang, X. Lu, Nano Energy 55 (2019) 447–453.
[92] P. Yang, X. Xu, Y. Li, D. Yong, P. Qiang, X. Tan, W. Mai, Z. Lin, W. Wu, T. Li, ACS Nano 7 (2013) 2617–2626.
[93] L.I. Wei, S. Jing, M. Chen, Nano Energy 3 (2014) 95–101.
[94] Y. Hu, J. Yang, Q. Jing, S. Niu, W. Wu, Z.L. Wang, ACS Nano 7 (2013) 10424–10432.
[95] Q. Jing, G. Zhu, W. Wu, B. Peng, Y. Xie, R.P.S. Han, L.W. Zhong, Nano Energy 10 (2014) 305–312.
[96] F.R. Fan, L. Lin, G. Zhu, W. Wu, R. Zhang, Z.L. Wang, Nano Lett. 12 (2012) 3109.

Chenxiang Ma received his B.S.in Chemical Engineering in 2013 from Tianjin University. He is currently pursuing his Ph.D. in School of Chemical Engineering and Technology at Tianjin University. He was a visiting student in Industrial Engineering at Purdue University from 2016 to 2018 under the supervision of Prof. Wenzhuo Wu. His research interests focus on the synthesis of nanomaterials for energy storage devices, and self-powered system

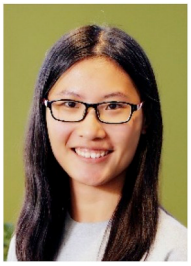

Ruoxing Wang received her BS degree in Chemistry in 2011 from University of Science and Technology of China (USTC). She is currently a PhD student in Industrial Engineering at Purdue University under the supervision of Prof. Wenzhuo Wu. Her research interests mainly focus on nanomanufacturing including the design of functional nanomaterials and fabrication of nanodevices for energy and human-health related applications

Halil Tetik received his B.S. and M.S. degree in mechanical engineering from Izmir Institute of Technology, Izmir, Turkey, in 2013 and 2016, respectively. He is now a Ph.D. student under the supervision of Prof. Dong Lin at industrial and manufacturing systems engineering, Kansas State University, USA. His present research interests mainly focus on additive manufacturing techniques for the fabrication of functional materials and devices

Shengjie Gao received his BS degree in Materials Chemistry from Lanzhou University, China in 2016. He is currently working towards his PhD degree at School of Industrial Engineering in Purdue University under the supervision of Dr. Wenzhuo Wu. His current research interests mainly focus on the semiconductor device fabrication, characterization of low-dimensional piezoelectric/ferroelectric materials, self-powered smart system and its application in Human-Computer Interface.

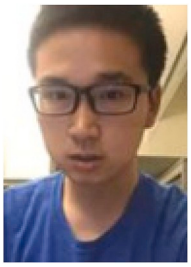

Min Wu received his B.S. in Materials Science and Engineering from the University of Science and Technology Beijing in 2014 and his M.S. in Mechanical and Energy Engineering from the University of North Texas in 2016. He is pursuing his Ph.D. in the School of Industrial Engineering at Purdue University under the supervision of Prof. Wenzhuo Wu. His research interest includes the synthesis of low-dimensional materials and investigation of their piezoelectric properties, nanodevice fabrication and flexible electronics.

Dr. Zhiyuan Tang is a professor in School of Chemical Engineering and Technology at Tianjin University. Dr. Tang received his B.S.in 1969 and his MS degree in 1981 in Chemical Engineering from Tianjin University. Dr. Tang's research interests include the materials design and preparation for lithium-ion batteries and safety issue control in the manufacturing process.

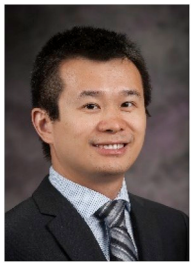

Dr Dong Lin is Assistant Professor in Department of Industrial and Manufacturing Systems Engineering at Kansas State University. He received his BS in Mechanical Engineering in 2004 from Harbin Institute of Technology, and his MS in Mechanical Engineering from Huazhong University of Science and Technology (2007) and University of Nebraska-Lincoln (2009). Dr Lin received his Ph.D. from Purdue University in Industrial Engineering. Dr Lin's research interests include additive manufacturing of 0D, 1D, and 2D aerogels for applications in energy, electronics, and wearable devices. He was a recipient of Guinness World's Record: The Least Dense 3D-printed Structure ($0.5\ mg\ cm^{-3}$) in 2018

Dong Ding is a senior staff engineer/scientist in the directorate of Energy and Environmental Science & Technology at Idaho National Laboratory, leading the efforts in the area of electrochemical processing and electrocatalysis at elevated temperatures. He received his doctorate in material science at the University of Science & Technology of China, where he also earned a bachelor's in materials chemistry. His current research interests include natural gas/natural gas liquids upgrading, solid oxide fuel cells and electrolysis cells, advanced manufacturing of solid oxide cells/stacks, integrated energy systems, CO_2 conversion, ammonia electrosynthesis, electrocatalysis, carbon & hydrocarbon engineering, batteries and supercapacitors.

Dr Wenzhuo Wu is the Ravi and Eleanor Talwar Rising Star Assistant Professor in School of Industrial Engineering at Purdue University. He received his BS in Electronic Information Science and Technology in 2005 from the University of Science and Technology of China (USTC), Hefei and his ME in Electrical and Computer Engineering from the National University of Singapore (NUS) in 2008. Dr Wu received his PhD from Georgia Institute of Technology in Materials Science and Engineering in 2013. Dr Wu's research interests include design, manufacturing, and integration of 1D and 2D nanomaterials for applications in energy, electronics, optoelectronics, and wearable devices. He was a recipient of the Oak Ridge Associated Universities (ORAU) Ralph E. Powe Junior Faculty Enhancement Award in 2016, the IOP Semiconductor Science and Technology Best Early Career Research in 2017, and the Society of Manufacturing Engineers (SME) Barbara M. Fossum Outstanding Young Manufacturing Engineer Award in 2019.